Acta Cryst A FOUNDATIONS ADVANCES

ISSN 2053-2733

Generalized Penrose tiling as a quasilattice for decagonal quasicrystal structure analysis

Maciej Chodyn,[a] Pawel Kuczera[b]* and Janusz Wolny[a]

[a]Faculty of Physics and Applied Computer Science, AGH University of Science and Technology, al. Mickiewicza 30, Krakow, Poland, and [b]Laboratory of Crystallography, ETH Zurich, Wolfgang-Pauli-Strasse 10, Zurich, CH-8093, Switzerland. *Correspondence e-mail: qczera@gmail.com

Received 25 August 2014
Accepted 13 November 2014

Keywords: decagonal quasicrystals; generalized Penrose tiling; average unit cell.

The generalized Penrose tiling is, in fact, an infinite set of decagonal tilings. It is constructed with the same rhombs (thick and thin) as the conventional Penrose tiling, but its long-range order depends on the so-called shift parameter ($s \in \langle 0; 1)$). The structure factor is derived for the arbitrarily decorated generalized Penrose tiling within the average unit cell approach. The final formula works in physical space only and is directly dependent on the s parameter. It allows one to straightforwardly change the long-range order of the refined structure just by changing the s parameter and keeping the tile decoration unchanged. This gives a great advantage over the higher-dimensional method, where every change of the tiling (change in the s parameter) requires the structure model to be built from scratch, *i.e.* the fine division of the atomic surfaces has to be redone.

1. Introduction

The structure analysis of decagonal quasicrystals (DQCs) is still a great challenge. Despite many years of efforts, the accuracy of structure refinements is far from that of periodic crystals. One of the important problems is determining the long-range order (LRO), that is, the right kind of decagonal tiling underlying the structure. Modern high-resolution electron microscopy can be helpful, but even the best quality images depict only a small fraction of the structure and hence no definite statement about the kind of tiling underlying the structure can be made. Two main approaches are used to tackle the structure refinement of DQCs: the higher-dimensional (nD) approach (de Wolff, 1974; Janssen, 1986; Takakura *et al.*, 2001; Cervellino *et al.*, 2002) and the average unit cell (AUC) approach (Wolny, 1998; Kozakowski & Wolny, 2010). The details of these methods are broadly discussed in the literature. However, both share a common problem. The first step of model building is to describe the structure in physical space in the framework of a pre-assumed tiling. Then, in the nD approach, the model has to be embedded in the higher-dimensional space to obtain the atomic surfaces in the perpendicular space. In the AUC approach the decoration of the unit tiles can be directly used for the structure-factor calculation. A vast majority of (if not all) models of DQCs in the literature are based on the Penrose mutual local derivability (PMLD) class of tilings (Baake *et al.*, 1991), *e.g.* pentagonal Penrose tiling, rhombic Penrose tiling, hexagon–star–boat tiling. The choice of a particular tiling from the PMLD class is a matter of convenience in the sense that the structural details may be more easily understood when described using one tiling then another. However, formally, the LRO for all PMLD class tilings is the same and if the structure is described by one tiling from the PMLD class it can also be described by

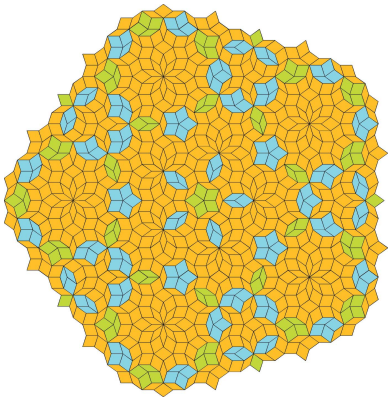

Table 1
The coordinates $(x_\perp, y_\perp)$ of ASs for $z_\perp = 1, 2, 3$ as a function of shift (s), $\alpha = (\tau + 2)^{1/2}/2$.

$z_\perp = 1$	$z_\perp = 2$	$z_\perp = 3$	$z_\perp = 4$	$z_\perp = 5$
$(1, 0) \cdot s$	$\left(1 + \frac{s}{2\tau}, -s\alpha\right)$	$\left(\frac{\tau^2}{2} + \frac{s}{2\tau}, \alpha - s\alpha\right)$	$\left(\tau - \frac{s\tau}{2}, s\frac{\alpha}{\tau}\right)$	$(-1, 0) \cdot (1 - s)$
$\left(-\frac{\tau}{2}, -\frac{\alpha}{\tau}\right) \cdot s$	$\left(1 + \frac{s}{2\tau}, s\alpha\right)$	$\left(\frac{\tau^2}{2} + \frac{s}{2\tau}, -\alpha + s\alpha\right)$	$\left(\tau - \frac{s\tau}{2}, -s\frac{\alpha}{\tau}\right)$	$\left(\frac{\tau}{2}, -\frac{\alpha}{\tau}\right) \cdot (1 - s)$
$\left(-\frac{\tau}{2}, \frac{\alpha}{\tau}\right) \cdot s$	$\left(\frac{1}{2\tau} + s, \alpha\right)$	$\left(\frac{\tau^2}{2} - \frac{s\tau}{2}, \alpha + s\frac{\alpha}{\tau}\right)$	$\left(\frac{1}{2} + \frac{s}{2\tau}, \tau\alpha - s\alpha\right)$	$\left(\frac{\tau}{2}, \frac{\alpha}{\tau}\right) \cdot (1 - s)$
$\left(\frac{1}{2\tau}, \alpha\right) \cdot s$	$\left(\frac{1}{2\tau} + s, -\alpha\right)$	$\left(\frac{\tau^2}{2} - \frac{s\tau}{2}, -\alpha - s\frac{\alpha}{\tau}\right)$	$\left(\frac{1}{2} + \frac{s}{2\tau}, -\tau\alpha + s\alpha\right)$	$\left(-\frac{1}{2\tau}, \alpha\right) \cdot (1 - s)$
$\left(\frac{1}{2\tau}, -\alpha\right) \cdot s$	$\left(\frac{1}{2\tau} - \frac{s\tau}{2}, \alpha + s\frac{\alpha}{\tau}\right)$	$\left(-\frac{1}{2} + s, -\tau\alpha\right)$	$\left(\frac{1}{2} - \frac{s\tau}{2}, \tau\alpha - s\frac{\alpha}{\tau}\right)$	$\left(-\frac{1}{2\tau}, -\alpha\right) \cdot (1 - s)$
	$\left(\frac{1}{2\tau} - \frac{s\tau}{2}, -\alpha - s\frac{\alpha}{\tau}\right)$	$\left(-\frac{1}{2} + s, \tau\alpha\right)$	$\left(\frac{1}{2} - \frac{s\tau}{2}, -\tau\alpha + s\frac{\alpha}{\tau}\right)$	
	$\left(-\frac{\tau}{2} + \frac{s}{2\tau}, \alpha + s\alpha\right)$	$\left(-\frac{1}{2} - \frac{s\tau}{2}, -\tau\alpha + s\frac{\alpha}{\tau}\right)$	$\left(-\frac{\tau^2}{2} + s, \alpha\right)$	
	$\left(-\frac{\tau}{2} + \frac{s}{2\tau}, -\alpha - s\alpha\right)$	$\left(-\frac{1}{2} - \frac{s\tau}{2}, \tau\alpha - s\frac{\alpha}{\tau}\right)$	$\left(-\frac{\tau^2}{2} + s, -\alpha\right)$	
	$\left(-\frac{\tau}{2} - \frac{s\tau}{2}, \frac{\alpha}{\tau} - s\frac{\alpha}{\tau}\right)$	$\left(-\frac{\tau^2}{2} + \frac{s}{2\tau}, s\alpha\right)$	$\left(-\frac{\tau^2}{2} + \frac{s}{2\tau}, -s\alpha\right)$	
	$\left(-\frac{\tau}{2} - \frac{s\tau}{2}, -\frac{\alpha}{\tau} + s\frac{\alpha}{\tau}\right)$	$\left(-\frac{\tau^2}{2} + \frac{s}{2\tau}, -s\alpha\right)$	$\left(-\frac{\tau^2}{2} + \frac{s}{2\tau}, s\alpha\right)$	

any other tiling from this class. Recently the rhombic Penrose tiling (PT) was used as a quasilattice in the AUC approach to describe a variety of different DQC phases (Kuczera *et al.*, 2011, 2012). However, it is an open question whether PMLD class tilings really describe their LRO in the best way.

PT can be easily generalized. The so-called generalized Penrose tiling (GPT) (Pavlovitch & Kleman, 1987; Ishihara & Yamamoto, 1988), in principle, does not belong to the PMLD class. The unit tiles of GPT are still the two Penrose rhombs and the local symmetry is preserved. However, its matching rules, and hence the tile arrangements, depend on a certain continuous parameter ($s \in \langle 0; 1)$). There is therefore an infinite set of different GPTs for different s values (GPT reduces to PT for $s = 0$) and by varying s the LRO of the tiling is changed. The diffraction properties of GPT have been studied before, *e.g.* Jarić (1986). The goal of this paper, however, is to derive a structure factor of arbitrarily decorated GPT in the AUC approach and show how the GPT concept can be practically applied for the refinement process of DQCs. The final formula should work in physical space only and be a function of the parameter s. This will allow one to change the LRO of the structural model with fixed unit tile decorations. Note that such an approach gives a great advantage over the nD approach. An nD model has to be constructed from scratch every time the tiling is changed (every time s is changed the atomic surfaces have to be repartitioned) and, hence, there is no way to optimize the s parameter in the refinement process.

2. Construction and matching rules of GPT

The easiest way to generate decagonal tilings is to project a five-dimensional hypercubic lattice (Steurer & Deloudi, 2009). The construction requires two five-dimensional bases called D and V. These two bases are rotated with respect to each other and can be related by the following equation:

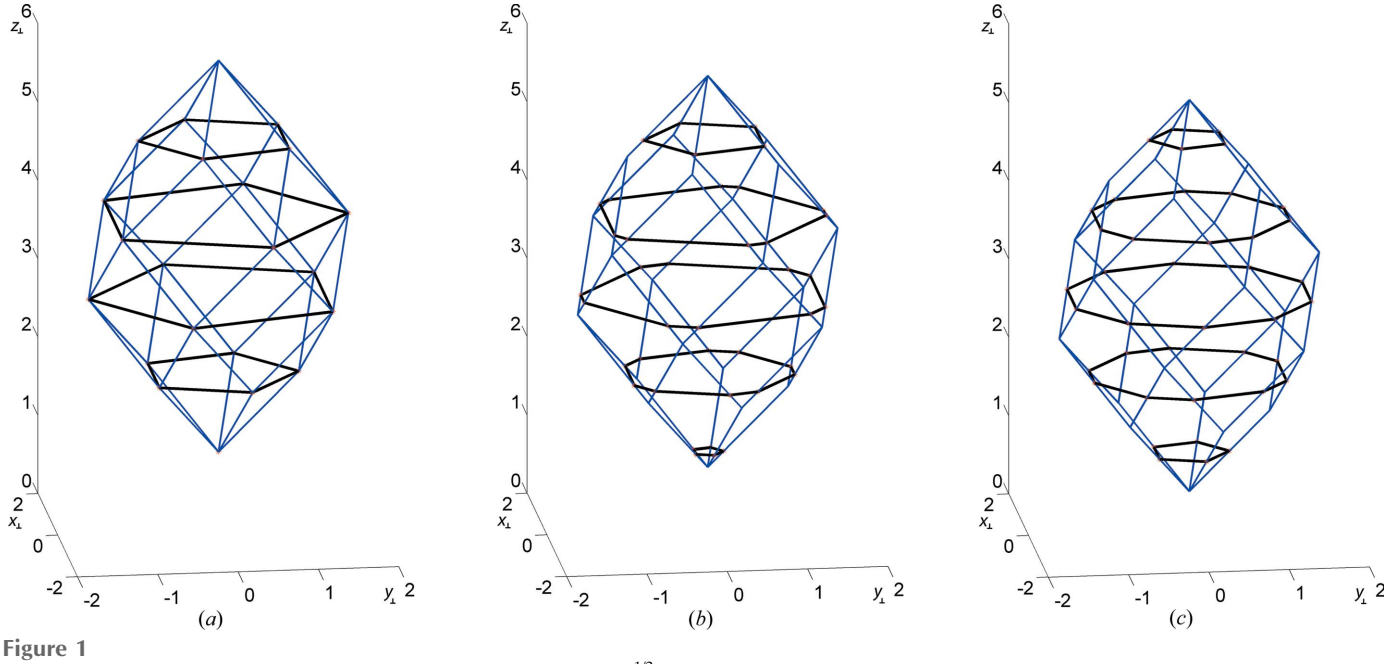

Figure 1
The ASs of PT (*a*), GPT $s = 0.2$ (*b*), GPT $s = 0.5$ (*c*). The factor $1/2^{1/2}$ on the z axis was omitted.

$$\begin{bmatrix} x_{\parallel} \\ y_{\parallel} \\ x_{\perp} \\ y_{\perp} \\ z_{\perp} \end{bmatrix}_V = a \begin{bmatrix} 1 & \cos(\frac{2\pi}{5}) & \cos(\frac{4\pi}{5}) & \cos(\frac{6\pi}{5}) & \cos(\frac{8\pi}{5}) \\ 0 & \sin(\frac{2\pi}{5}) & \sin(\frac{4\pi}{5}) & \sin(\frac{6\pi}{5}) & \sin(\frac{8\pi}{5}) \\ 1 & \cos(\frac{4\pi}{5}) & \cos(\frac{8\pi}{5}) & \cos(\frac{12\pi}{5}) & \cos(\frac{16\pi}{5}) \\ 0 & \sin(\frac{4\pi}{5}) & \sin(\frac{8\pi}{5}) & \sin(\frac{12\pi}{5}) & \sin(\frac{16\pi}{5}) \\ 1/2^{1/2} & 1/2^{1/2} & 1/2^{1/2} & 1/2^{1/2} & 1/2^{1/2} \end{bmatrix} \times \begin{bmatrix} x_0 \\ x_1 \\ x_2 \\ x_3 \\ x_4 \end{bmatrix}_D . \quad (1)$$

The matrix in the above equation is traditionally called the W matrix. In the V basis the five-dimensional space can be decomposed to two orthogonal subspaces: two-dimensional parallel space (par-space, $V_{\parallel}$) and three-dimensional perpendicular space (perp-space, $V_{\perp}$). PT is obtained by projecting a five-dimensional hypercubic lattice on the par-space through a window consisting of four pentagons (and one additional point) in perp-space. These four pentagons are called atomic surfaces (ASs) and their vertices are obtained by projecting one unit cell of the five-dimensional hypercubic lattice on perp-space (Fig. 1*a*). The vertices of the AS form a rhombicosahedron in perp-space. In other words, only a subset of points of the five-dimensional hypercubic lattice, whose projection on the perp-space lies within the ASs, is projected on the par-space to form PT. Such a subset of points lies within a 'projection strip' in five-dimensional space. If such a projection strip is shifted by a fraction of a unit vector, the coordinates of the rhombicosahedron will change. Points of the five-dimensional hypercubic lattice projected on perp-space will now intersect the rhombicosahedron at different heights, resulting in a change of shape of ASs (Figs. 1*b*, 1*c*). This is equivalent to a shift of the AS in Fig. 1(*a*) along the body diagonal of the rhombicosahedron. Three of the previously pentagonal ASs will become decagons (equilateral only for the shift equal to 0.5), one will remain pentagonal, and additionally one more pentagon will be created (for PT it is a single point). The exact coordinates of ASs as a function of s are presented in Table 1. A projection of the five-dimensional hypercubic lattice through a window consisting of these five polygons will generate the GPT whose structure will depend on the shift parameter s.

The GPT is built out of two rhombs, like the regular PT. Examples of GPT structures with a different shift parameter are shown in Fig. 2. It is clear that PT matching rules cannot be applied to GPT. The seven possible vertex configurations (if matching rules are neglected) of PT are shown in Fig. 3. New vertex configurations for GPT are the result of the existence of an additional AS, and the change of shape of remaining ASs. As an example, additional possible vertex configurations for shift parameter 0.2 and 0.5 are shown in Fig. 4. It is important to note that different sets of vertex configurations will be created for each value of the shift parameter. That is essentially why every value s gives a different LRO of the resulting structure. The ratio of the number of L and the number of S rhombs remains unchanged and, as for PT, is equal to τ.

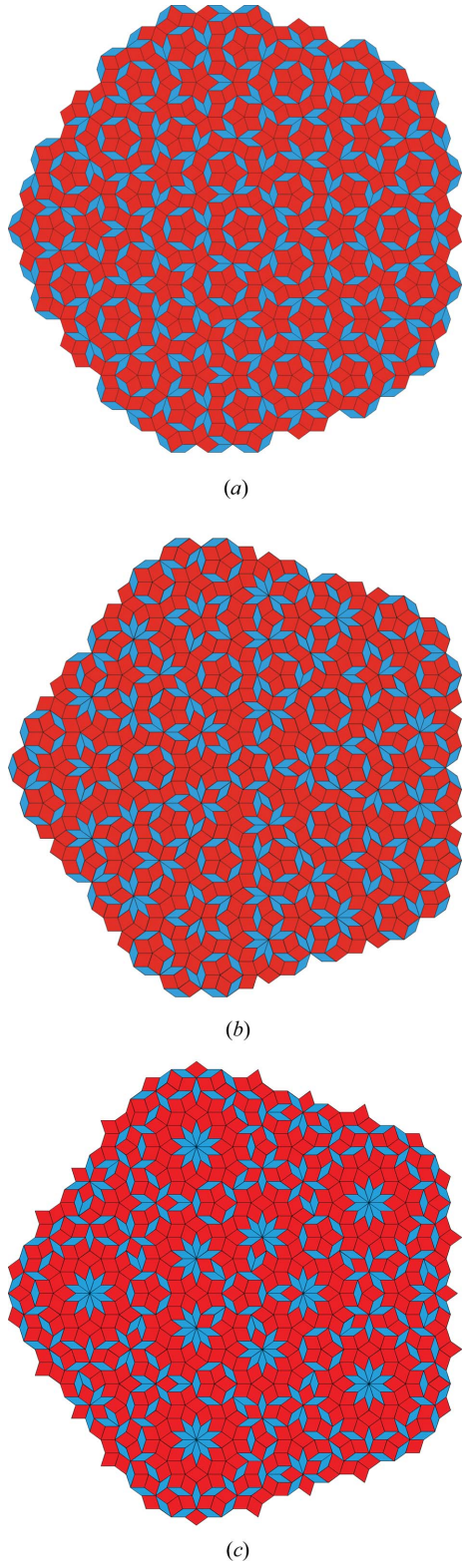

(*a*)

(*b*)

(*c*)

Figure 2
Generalized Penrose tilings for different shift parameters: (*a*) $s = 0$, (*b*) $s = 0.2$ and (*c*) $s = 0.5$.

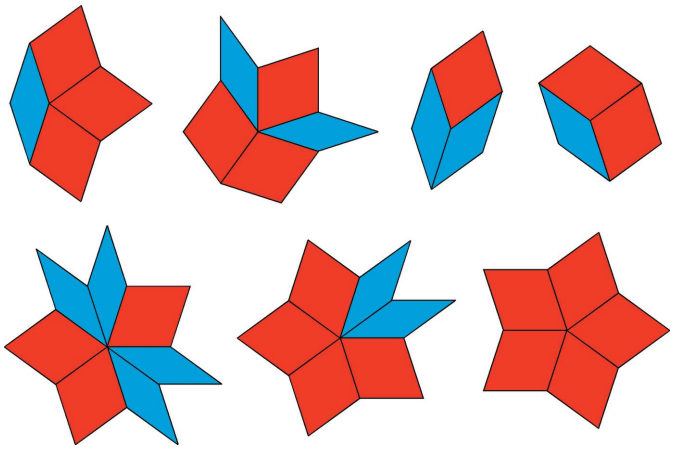

Figure 3
Seven possible rhomb configurations for PT (matching rules neglected).

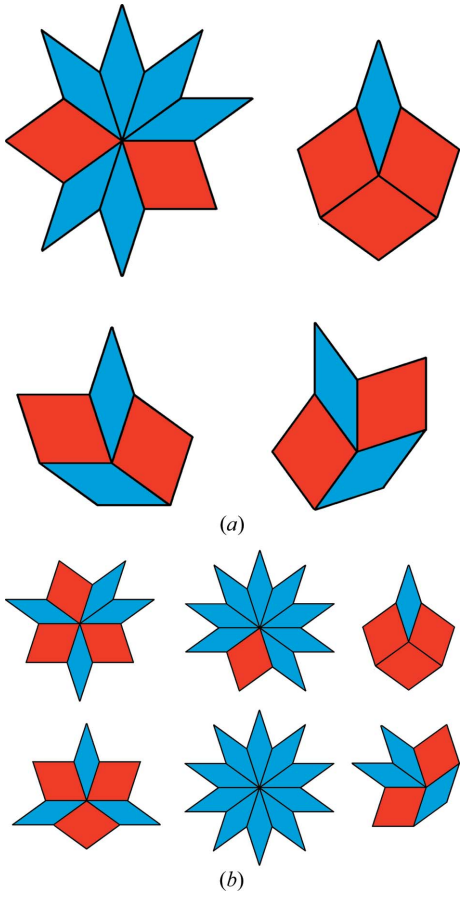

Figure 4
Examples of new rhomb configurations for GPT, $s = 0.2$ (a) and $s = 0.5$ (b).

3. Density distribution

Both PT and GPT have the same building units, *i.e.* thick (L) and thin (S) rhombs. Each of these rhombs can have five distinct orientations. In Fig. 5 one L rhomb is depicted in $V_{\parallel}$ subspace and projected along $z_{\perp}V_{\perp}$ subspace. (Note that the shape of an L rhomb in $V_{\perp}$ subspace projected along the $z_{\perp}$ direction is the same as the shape of an S rhomb in $V_{\parallel}$ subspace. An analogous statement is true for the shape of an S rhomb.) Any edge of any rhomb (L or S) can always be described as a projection of a D-space basis vector. The D-space coordinates of appropriate basis vectors are given in Fig. 5. We will represent the L rhomb in Fig. 5 by one of its vertices (A) and find out what are the possible locations of A on the ASs. Four ASs (and one additional point as in Fig. 1) of ordinary PT have five consecutive integer values of the $z_{\perp}$ coordinate (they are obtained by projection of one unit cell of the five-dimensional hypercubic lattice). Without the loss of generality, we can assume that these coordinates are $1, 2, \ldots, 5$ [at $z_{\perp} = 1$ a single point is located (see Fig. 1a)]. It is easy to see that point A of the rhomb in Fig. 5 can only be located at $z_{\perp} = 2$ or at $z_{\perp} = 3$. It is so because the $z_{\perp}$ coordinate is increased by 1 for points B and C and by 2 for point D [see equation (1) (neglecting the normalizing factors $2^{1/2}$)]. Since the area at $z_{\perp} = 1$ is zero, these are the only possibilities. An analogous statement is valid for L and S rhombs in any orientation. We can conclude that in PT there are two different families of L and S rhombs with five orientations each. One family with rhomb vertices located at $z_{\perp} = 2, 3, 4$ and the other with rhomb vertices located at $z_{\perp} = 3, 4, 5$. In the structure model, the atomic decoration of rhombs from different families can be the same, but does not have to be. Note, however, that if the decoration is different, the symmetry is decreased to pentagonal. For GPT the AS at $z_{\perp} = 1$ is no longer a single point (Figs. 1b, 1c). It follows that in the GPT there are three distinct families of rhombs. The additional family can have vertices located at $z_{\perp} = 1, 2, 3$. Again, in principle, the decoration of each of the three families could be different. In Fig. 6 the GPT structures from Fig. 2 have been coloured in such a way that each family of rhombs is marked with a different colour.

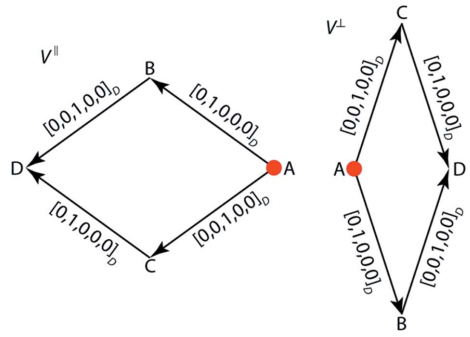

Figure 5
An example L rhomb in $V_{\parallel}$ subspace and $V_{\perp}$ subspace projected along the $z_{\perp}$ direction.

The next step is to find out where exactly the point A of a given kind of rhomb from a given family in a given orientation can be located on the respective AS. An example construction for an L rhomb (oriented as in Fig. 5) from a family at $z_{\perp} = 2$, 3, 4 is shown in Fig. 7. Point A at $z_{\perp} = 2$ can only take such positions that points B and C at $z_{\perp} = 3$ and point D at $z_{\perp} = 4$ stay inside their respective ASs. The searched distribution has a triangular shape for PT and is hexagonal for GPT. An analogous construction can be done for any rhomb in any orientation and from any family. It is worth mentioning that the distributions for families $z_{\perp} = 1, 2, 3$ and $z_{\perp} = 3, 4, 5$ will

always be triangular for both PT and GPT. This is because the ASs at $z_\perp = 1$ and $z_\perp = 5$ are pentagonal for both PT and GPT. It is also important to note that it is enough to get the distribution for one orientation of a given rhomb from a given family. The rest can be obtained by rotation. The consecutive orientations of rhombs in $V_\parallel$ subspace are related by multiples of $2\pi/5$; the consecutive orientations of the distributions in $V_\perp$, however, are related by multiples of $4\pi/5$ [see equation (1)]. The distribution of point A for L and S rhombs oriented as in Fig. 8 for all three families of rhombs is given in Table 2. As mentioned before, the distributions of other orientations from a given family can be obtained by proper rotations.

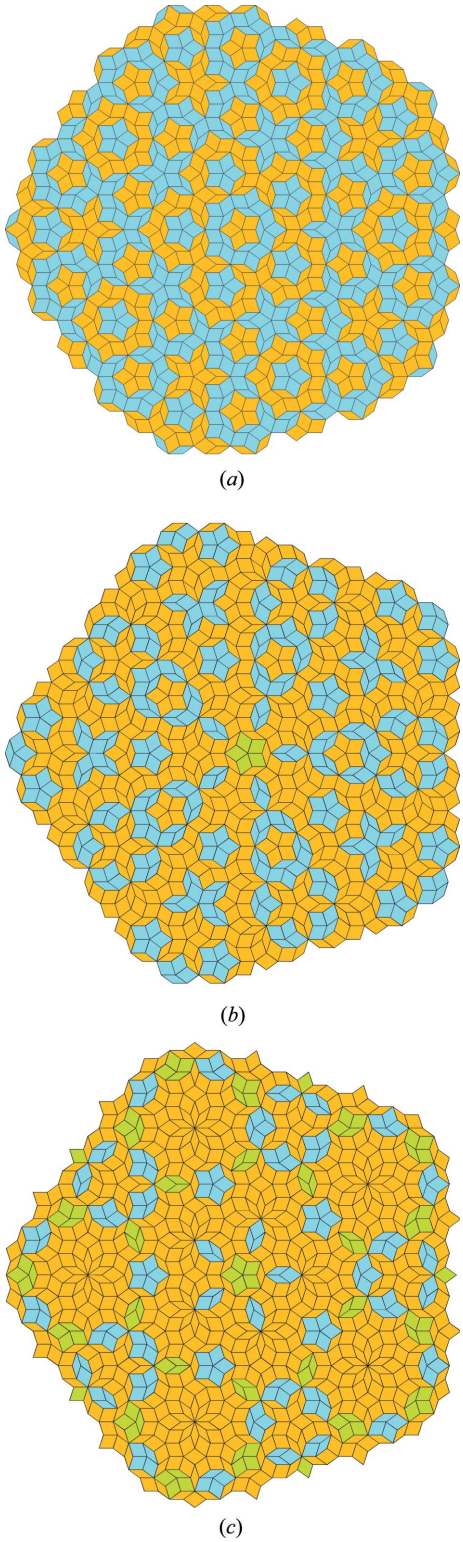

Figure 6
Distribution of rhomb families in physical space for PT (*a*), GPT $s = 0.2$ (*b*) and GPT $s = 0.5$ (*c*). The family based on $z_\perp = 1, 2, 3$ is coloured in green, $z_\perp = 2, 3, 4$ in yellow and $z_\perp = 3, 4, 5$ blue.

4. Structure factor

The derivation of the structure factor for an arbitrarily decorated GPT using the AUC is done similarly to that of the structure factor of decorated PT (Kozakowski & Wolny, 2010). We will only sketch the derivation here. For a decorated GPT we can write the electron density as

$$\rho_{\mathrm{GPT}} = \sum_{T=\{L,S\}} \sum_{f=1}^{3} \sum_{\theta=1}^{5} \rho^{\mathrm{lattice}}_{T_{f,\theta}} \rho^{\mathrm{tile}}_{T_{f,\theta}}. \qquad (2)$$

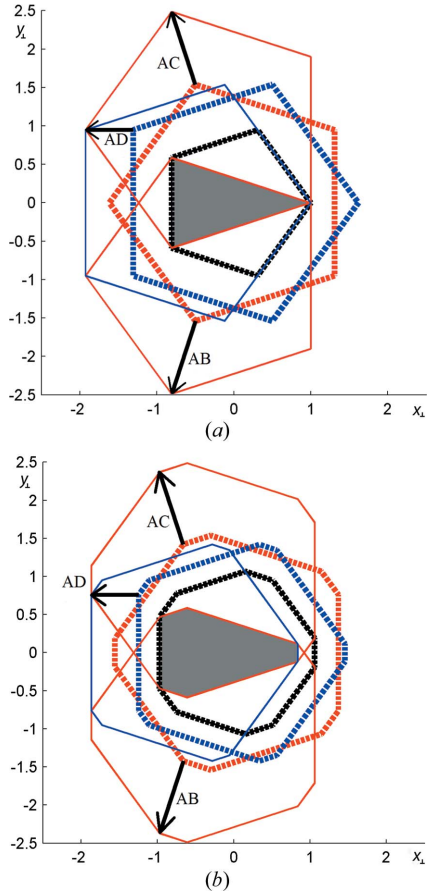

Figure 7
The procedure of obtaining the distribution shape (grey region) of PT (*a*) and GPT, $s = 0.2$ (*b*). Thick dashed lines indicate the ASs at $z_\perp = 2$ (black), $z_\perp = 3$ (red) and $z_\perp = 4$ (blue). Thin solid lines are ASs shifted in the $(x_\perp, y_\perp)$ plane by the following vectors: $AB = [-0.5(\tau - 1), -0.5(\tau + 2)^{1/2}, 1]$, $AC = [-0.5(\tau - 1), 0.5(\tau + 2)^{1/2}, 1]$, $AD = (-\tau + 1, 0, 2)$. The grey regions at $z_\perp = 2$ show all possible locations of point A of the L rhomb oriented as in Fig. 5 such that the points B, C ($z_\perp = 3$) and D ($z_\perp = 4$) stay within their respective ASs.

Table 2
The coordinates (x_P, y_P) of polygon areas as a function of shift(s) of the GPT atomic surfaces, which describe the distribution of the chosen thick and thin rhomb [$\alpha = (\tau+2)^{1/2}/2$].

	Thick rhomb	Thin rhomb
$z_\perp = 1$	$(s, 0)$	$(s, 0)$
	$\left(-\frac{s\tau}{2}, \frac{s\alpha}{\tau}\right)$	$\left(\frac{s}{2\tau}, \alpha\right)$
	$\left(-\frac{s\tau}{2}, -\frac{s\alpha}{\tau}\right)$	$\left(\frac{s}{2\tau}, -\alpha\right)$
$z_\perp = 2$	$\left(-\frac{\tau}{2}-\frac{s\tau}{2}, \frac{\alpha}{\tau}-s\frac{\alpha}{\tau}\right)$	$\left(\frac{1}{2\tau}+\frac{s}{2\tau}, \alpha-s\alpha\right)$
	$\left(-\frac{\tau}{2}+s, \frac{\alpha}{\tau}\right)$	$\left(\frac{1}{2\tau}+s, \alpha\right)$
	$\left(1-\frac{s\tau}{2}, s\alpha\right)$	$\left(1+\frac{s}{2\tau}, s\alpha\right)$
	$\left(1-\frac{s\tau}{2}, -s\alpha\right)$	$\left(1+\frac{s}{2\tau}, -s\alpha\right)$
	$\left(-\frac{\tau}{2}+s, -\frac{\alpha}{\tau}\right)$	$\left(\frac{1}{2\tau}+s, -\alpha\right)$
	$\left(-\frac{\tau}{2}-\frac{s\tau}{2}, -\frac{\alpha}{\tau}+s\frac{\alpha}{\tau}\right)$	$\left(\frac{1}{2\tau}+\frac{s}{2\tau}, -\alpha+s\alpha\right)$
$z_\perp = 3$	$(-\tau+s, 0)$	$\left(\frac{1}{\tau}+s, 0\right)$
	$\left(1-\frac{\tau}{2}-\frac{s\tau}{2}, -\frac{\alpha}{\tau}+\frac{s\alpha}{\tau}\right)$	$\left(\frac{\tau^2}{2}+\frac{s}{2\tau}, -\alpha+s\alpha\right)$
	$\left(1-\frac{\tau}{2}-\frac{s\tau}{2}, \frac{\alpha}{\tau}-\frac{s\alpha}{\tau}\right)$	$\left(\frac{\tau^2}{2}+\frac{s}{2\tau}, \alpha-s\alpha\right)$

There are two kinds of rhombs [L and S – sum over T in equation (2)], grouped in the three distinct families (sum over f), and each of the rhombs in each family can be found in GPT in five different orientations (sum over θ). Having this in mind, we can describe the electron density of an arbitrarily decorated GPT as summed up convolutions of sublattices of a given kind of rhomb from a given family in a given orientation ($\rho^{\rm lattice}_{T_{f,\theta}}$) and the electron density inside a particular rhomb ($\rho^{\rm tile}_{T_{f,\theta}}$). Note that the decoration of each kind of rhomb in a given family is the same (properly rotated for different orientations). The structure factor is simply a Fourier transform (FT) of the electron density in equation (2):

$$\mathrm{FT}(\rho_{\rm GPT}) = \sum_{T=\{L,S\}} \sum_{f=1}^{3} \sum_{\theta=1}^{5} \mathrm{FT}(\rho^{\rm lattice}_{T_{f,\theta}}) \cdot \mathrm{FT}(\rho^{\rm tile}_{T_{f,\theta}}). \qquad (3)$$

The FT of the electron-density distribution inside a given tile is just an ordinary sum of exponential factors – like for a periodic crystal:

$$\mathrm{FT}(\rho^{\rm tile}_{T_{f,\theta}}) = \sum_{j}^{n_{T_{f,\theta}}} p_j f_a^j \exp(i\mathbf{k}_{\mathbf{n},\mathbf{m}} \cdot \mathbf{r}_j^{T_\theta}), \qquad (4)$$

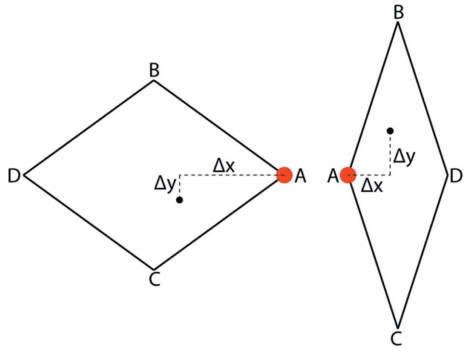

Figure 8
Example L and S rhombs. The distributions listed in Table 2 are given for these orientations of L and S rhombs. The red dot indicates the 'rhomb representing point'. The relative coordinates of points decorating the structure units are calculated with respect to this point.

where $n_{T_{f,\theta}}$ is the number of atoms decorating the structure unit $T_{f,\theta}$, $\mathbf{r}_j^{T_\theta}$ is the position (in par-space) of a given atom in a structural unit with respect to the representing point A (Fig. 8), and $\mathbf{k}_{\mathbf{n},\mathbf{m}}$ is a reciprocal-lattice vector written using $(\mathbf{n}, \mathbf{m})$ indices (Kozakowski & Wolny, 2010). Assuming that a is the rhomb's edge length, one writes

$$k_x = \frac{2\pi}{5a}\left[(n_1+n_2) + \frac{(m_1+m_2)}{\tau}\right],$$
$$k_y = \frac{2\pi}{5a}\tau(\tau+2)^{1/2}\left[(n_1-n_2) + \frac{(m_1-m_2)}{\tau}\right]. \qquad (5)$$

f_a^j is the atomic scattering factor of a given atom, p_j is the fraction of an atom inside the structure unit ($p_j = 1$ for atoms inside the rhombs, $p_j = 0.5$ at the edges, at the vertices $p_j = \frac{\varphi}{2\pi}$ where φ is the angle between the edges forming the vertex). The FT of the sublattice reads

$$\mathrm{FT}(\rho^{\rm lattice}_{T_{f,\theta}}) = \exp[i\varphi(z_\perp^A)] \int\limits_{\mathrm{AUC}(T_{f,\theta})} \exp[i(\boldsymbol{\kappa}_{\mathbf{n},\mathbf{m}} \cdot \mathbf{u})]\,\mathrm{d}\mathbf{u}, \qquad (6)$$

where

$$\varphi(z_\perp^A) = -\frac{4\pi}{5}[(n_1+n_2) - 0.5(m_1+m_2)]z_\perp^A,$$
$$\kappa_x = \frac{2\pi}{5}[(n_1+n_2) - \tau(m_1+m_2)],$$
$$\kappa_y = \frac{2\pi}{5}\tau(\tau+2)^{1/2}[(n_1-n_2) - \tau(m_1-m_2)].$$

The integral in equation (6) runs over the AUC distribution of point A representing a given rhomb $T_{f,\theta}$. It is obtained by an oblique projection ($u_x = -\tau^{-2}x_\perp, u_y = -\tau^{-2}y_\perp$) of the distributions found in §3 and listed in Table 2, and $\boldsymbol{\kappa}_{\mathbf{n},\mathbf{m}}$ is a rescaled wavevector in the FT [the rescaling arises due to the oblique projection and scaling properties of PMLD tilings (Kozakowski & Wolny, 2010, Appendix A)]. Note that the value of $z_\perp^A$ can only be 1, 2 or 3, depending on the family of rhombs. The structure factor is a function of the shift parameter s. It enters the formula through the coordinates of the distributions in Table 2.

5. Test results

The formula derived in the previous paragraph was tested in two ways. In the first test we compared the diffraction intensities obtained in the AUC approach with the diffraction intensities obtained in the standard nD approach (by integration over the ASs). The tests were performed for multiple values of s. All the rhombs were decorated at the vertices. The results obtained in the AUC approach and in the nD approach are fully equivalent. In the second step, we tested the formula for an arbitrary decoration. All the rhombs were decorated at the vertices. Additionally, the family of rhombs $z_\perp = 1, 2, 3$ (the additional family that occurs only for GPT) was decorated at $(-1, 0.25)$ for the L rhomb and at $(1/2\tau, 0.5)$ for the S rhomb. The shift parameter s was set to 0.5. We calculated the FT and then the inverse FT to get the electron-density distribution. The results are shown in Fig. 9. All the maxima at the rhomb vertices are numbered with an appropriate $z_\perp$

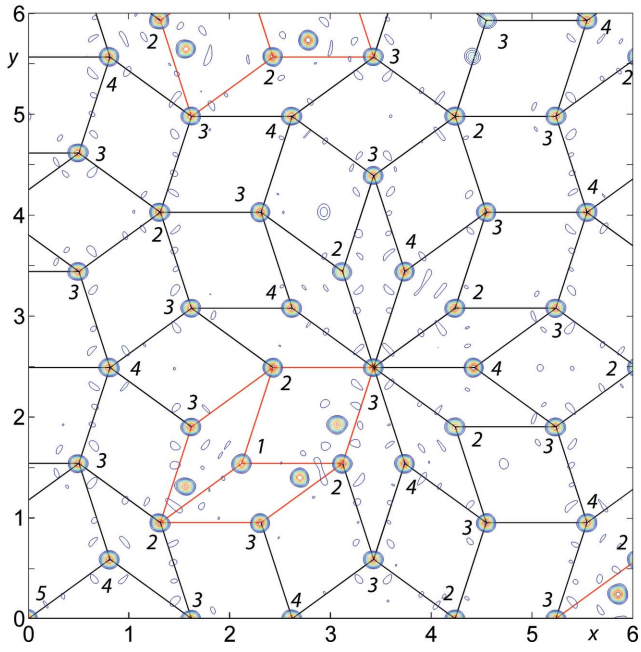

Figure 9
Electron density obtained from an inverse Fourier transform of the diffraction pattern for GPT with $s = 0.5$, decorated in vertices of building units, and with additional decoration in rhombs originating from new AS. Around 2.8 million peaks were used for the calculation, reciprocal-lattice vector range of $|\mathbf{k}| \in \langle 0; 35)$, background cutoff at 9% of the maximum electron-density value. Numbers written in italics indicate the $z_\perp$ coordinate of the AS from which the point originates.

coordinate. The family $z_\perp = 1, 2, 3$ (marked in red) is clearly additionally decorated at the assumed points. Fig. 10 shows the diffraction pattern of GPT with $s = 0.5$ with and without the additional decoration of the family $z_\perp = 1, 2, 3$. The additional decoration breaks mirror symmetry of the rhombs and hence the Laue class is reduced from 10/*mmm* (Fig. 10*a*) to 10/*m* (Fig. 10*b*) (assuming a three-dimensional structure consisting of GPT layers stacked periodically one above another).

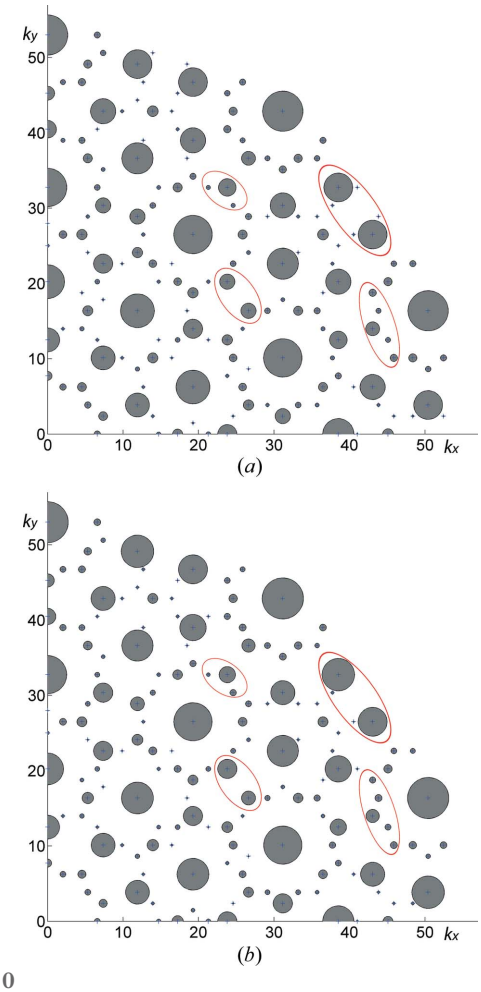

Figure 10
GPT diffraction pattern, $s = 0.5$, without (*a*) and with (*b*) the additional decoration of the rhomb family $z_\perp = 1, 2, 3$. The Laue symmetry is reduced from 10/*mmm* (*a*) to 10/*m* (*b*). Crosses indicate peak positions. Ellipses were used to indicate the regions of the diffraction pattern where the peak intensities change and the 10/*mmm* symmetry is broken.

6. Summary

We have shown the construction of the GPT and described the process of finding distributions of points representing rhombs in the AUC approach. Once these distributions are defined, the structure-factor calculation becomes trivial and essentially resembles the analogous calculation for periodic crystals. The final formula was subjected to various tests and proved to be correct. GPT is potentially an attractive alternative for building models of DQCs. The possibility to continuously change the LRO with just one parameter should make it feasible to attempt to fit the LRO during the refinement process of DQCs. In this case the AUC approach gives a tremendous advantage over the *n*D method because the structure factor directly depends on the shift parameter. In turn, in the *n*D approach, every change of the shift parameter practically requires a fresh repartitioning of ASs. An attempt to make the fine partitioning of ASs in the DQC model dependent on the *s* parameter, though in principle possible, would be incredibly complex. Additionally, for every change in the physical space model (*e.g.* atomic coordinate shift), this complex model would have to be changed. In the AUC approach the change in the physical space model yields a simple change in the decoration of the tiles.

Acknowledgements

This project has been partially supported by the Polish National Science Centre (NCN) under grant No. DEC-2013/11/B/ST3/03787 and by the Swiss National Science Foundation under grant No. 200021-153559.

References

Baake, M., Scholottmann, M. & Jarvis, P. D. (1991). *J. Phys. A Math. Gen.* **24**, 4637–4654.
Cervellino, A., Haibach, T. & Steurer, W. (2002). *Acta Cryst.* B**58**, 8–33.
Ishihara, K. N. & Yamamoto, A. (1988). *Acta Cryst.* A**44**, 508–516.
Janssen, T. (1986). *Acta Cryst.* A**42**, 261–271.
Jarić, M. (1986). *Phys. Rev. B*, **34**, 4685–4698.

Kozakowski, B. & Wolny, J. (2010). *Acta Cryst.* A**66**, 489–498.
Kuczera, P., Wolny, J., Fleischer, F. & Steurer, W. (2011). *Philos. Mag.* **91**, 2500–2509.
Kuczera, P., Wolny, J. & Steurer, W. (2012). *Acta Cryst.* B**68**, 578–589.
Pavlovitch, A. & Kleman, M. (1987). *J. Phys. A Math. Gen.* **20**, 687–702.
Steurer, W. & Deloudi, S. (2009). *Crystallography of Quasicrystals, Springer Series in Materials Science*, Vol. 126. Heidelberg, Dordrecht, London, New York: Springer.
Takakura, H., Yamamoto, A. & Tsai, A. P. (2001). *Acta Cryst.* A**57**, 576–585.
Wolff, P. M. de (1974). *Acta Cryst.* A**30**, 777–785.
Wolny, J. (1998). *Philos. Mag. A*, **77**, 395–412.